

Extraction of binary neutron star gravitational wave waveforms from Einstein Telescope using deep learning

CunLiang Ma,^{1,2} XinYao Yu,¹ Zhoujian Cao^{*,3,4,†} and Mingzhen Jia^{1,2}

¹*School of Information Engineering, Jiangxi University of Science and Technology, Ganzhou, 341000, China*

²*Jiangxi Provincial Key Laboratory of Multidimensional Intelligent Perception and Control, Ganzhou, 341000, China*

³*Institute of Applied Mathematics, Academy of Mathematics and Systems Science,*

Chinese Academy of Sciences, Beijing 100190, China

⁴*School of Fundamental Physics and Mathematical Sciences,*

Hangzhou Institute for Advanced Study, UCAS, Hangzhou 310024, China

In the future, the third generation (3G) gravitational wave (GW) detectors, exemplified by the Einstein Telescope (ET), will be operational. The detection rate of GW from binary neutron star (BNS) is expected to reach approximately 10^4 per year. To address the challenges posed by BNS GW data processing for 3G GW detectors, this paper explores the extraction of BNS waveforms from ET. Drawing inspiration from SPIIR's matched filtering approach, we introduce a novel framework leveraging deep learning for BNS waveform extraction. By integrating denoised outputs of time-delayed strain, we can reconstruct the embedded BNS waveform. We have established three distinct BNS GW denoising models, each tailored to address the early inspiral, later inspiral, and merger phases of BNS GW, respectively. To further regulate the waveform shape, we propose the Amplitude Regularity Model that takes denoised output as input and regulated waveform as output. The experiments conducted on test data demonstrate the efficacy of the denoising models, the Amplitude Regularity Models, as well as the overall waveform construction method. To the best of our knowledge, this marks the first instance of deep learning being utilized for the task of BNS waveform extraction. We believe that the proposed method holds promise for early warning, searching, and localization of BNS GWs.

I. INTRODUCTION

After conducting the initial three observation runs, the International Gravitational-wave Network (IGWN) [1] has accurately detected more than 90 confident gravitational wave (GW) events [2–5]. Among the confidently detected GW events, GW170817 and GW190425 specifically stem from the merging of binary neutron stars (BNSs). Meanwhile, other confidently identified events originate from either binary black hole (BBH) or neutron star-black hole (NSBH) mergers.

The observation of GW170817 was witnessed both in GW and electromagnetic spectra [6, 7]. This groundbreaking observation ushered in the dawn of Multi-Messenger Astrophysics that leverages observations across electromagnetic radiation, gravitational waves, cosmic rays, and neutrinos. GW170817 furnished conclusive proof that BNSs are one of the driving force behind short gamma ray bursts, marking the first direct evidence of this phenomenon, and it definitively established that GWs propagate at speeds virtually indistinguishable from that of light [8]. Most importantly, the discovery of GW170817 has played a pivotal role in illustrating that gravitational wave observations have the potential to deduce the tidal deformability of neutron stars [9–11].

Conventional GW search methods primarily rely on a

technique called template matched filtering [12–17]. This approach typically employs a template bank with extensive waveforms, each distinguished by various compact binary parameters, including but not limited to component masses and/or spins. Specifically, GW searches employing matched filtering techniques are currently focused on a distinct segment of the available parameter space. As mentioned in the literature [18], the main emphasis is on a 4D parameter space, which represents compact binary sources where the spin-aligned components orbit in quasi-circular paths.

In the future, third-generation (3G) detectors, such as Einstein Telescope (ET) [19] and Cosmic Explorer (CE) [20], will work. These detectors promise remarkable sensitivity advancements [21], elevating it by an order of magnitude. Furthermore, they are expected to considerably widen the bandwidth, reaching both lower and higher frequencies. In these cases, GW detectors have the potential to explore a broader 9D parameter space. In such a scenario, the computational demands of these low-latency GW searches will be exceedingly high, potentially posing significant challenges.

To address the computational efficiency challenge, numerous studies have concentrated on leveraging deep learning for GW searches [22–37]. In the case of the BNS merger, search efficiency holds utmost importance due to the critical need for swift follow-up observations to successfully detect their electromagnetic counterparts. Several studies have shown that deep learning can be efficiently used to search for BNS mergers [38–44], specifically in detecting pre-merger alerts from GWs emitted by BNSs [45–47]. The application of deep learning in this

*corresponding author

†Zhoujian Cao: zjcao@amt.ac.cn

context has been thoroughly explored, demonstrating its potential in identifying such events.

All BNS GW searches based on deep learning employ an end-to-end classification approach. Alternatively, the matched filtering method for BNS GW searches has the capability to exhibit the fluctuation of the signal-to-noise ratio (SNR) over time. Furthermore, the output generated through matched filtering can facilitate subsequent endeavors, such as source localization [48]. On the other hand, GW search methods based on end-to-end classification often face difficulties in providing the prior information required for tasks such as wave source localization and parameter estimation. The traditional matched filtering for BNS GW detection also faces challenges. Even a minor alteration in BNS masses can result in a significant waveform mismatch in this area, primarily due to the increased number of cycles within the frequency band that require precise alignment.

Fortunately, in 2023, a new task for envelope extraction was proposed, capable of predicting the hidden gravitational wave signal's envelope [49]. This task was employed to further validate search results by comparing the coalescence times across various detectors. Typically, most deep learning-based detection methods treat all time segments, regardless of whether they contain gravitational wave information, equally. However, recently, we leveraged the envelope extraction network to identify significant data segments. Subsequently, we utilized these key segments to predict templates using denoising [50]. These predicted templates then facilitated matched filtering. The denoising of BBH case has undergone extensive research [51–54]. Therefore, the framework can be conveniently utilized for BBH search. Currently, there is no existing research on denoising techniques specifically designed for BNSs. As a result, the application of the MSNRnet framework for BNS searching remains challenging.

If the denoising process can accurately predict the BNS GW template, the waveform mismatch issue inherent in matched filtering will be effectively resolved. Template prediction is just one among several applications of BNS GW denoising. The GW waveforms emitted by the BNS system carry vital information about the internal structure of neutron stars, reflected through the tidal deformability parameter, which is dependent on the equation of state of the neutron star. Additionally, the denoised BNS GW output aids in exploring the deformability of neutron stars.

In this study, we concentrate primarily on addressing the denoising challenge posed by binary neutron stars. It's crucial to note that denoising techniques developed for BBH cannot be seamlessly applied to BNS. This is primarily due to distinct characteristics inherent to each type of binary system. For instance, BBH signals typically last less than 2 seconds within the detector's sensitivity range, whereas BNS signals can persist for over 100 seconds. Additionally, the GW emitted during a BNS merger have a higher peak frequency compared to

those from a BBH merger. Furthermore, given the same matched filtering SNR, the peak amplitude of GW from a BNS is notably weaker than that of a BBH.

For the greater challenge of GW data processing in the future 3G detectors, in this work we focus on the BNS waveform construction based on 3G detectors taking ET as an example. The ET will enable us to embark on an exploration of the Universe through GWs, tracing its cosmic history all the way back to the cosmological dark ages. This groundbreaking endeavor promises to illuminate unresolved issues in fundamental physics and cosmology. The ET is expected to have a detection rate of approximately 10^4 to 10^6 events per year for BBHs and 7×10^4 events per year for BNSs [55, 56]. Recently, the detection of GW data from ET using deep learning methods has garnered significant attention, including BBH [57, 58] and Cosmic String Cusps [59].

For the long time-duration and high peak frequency of the BNS signal, in terms of computational complexity, it is virtually impossible to denoise all information from a deep learning model directly. Motivated by the template bank construction methods of traditional matched filtering pipelines SPIIR, we propose a new framework for BNS waveform construction. The SPIIR construct the template via summation of time shifted infinite impulse response (IIR) filters. In our framework we construct the waveform by combine of time shifted denoising results by different deep filters. Three sub-models (deep filters) are used for the overall waveform construction task. The first model pertains to the early inspiral phase of the signal, the second model focuses on the later inspiral stage of the signal, while the third model focuses on near merger stage that encompasses the inspiral leading up to the merger, the merger itself, and the subsequent ringdown stages of the BNS signal. We believe that the denoising model specifically designed for the early inspiral phase can serve as an early warning system for BNS events. Additionally, the comprehensively constructed waveform can be effectively utilized for template creation.

The sampling frequencies of our different denoising models are tailored to the specific frequency ranges of each stage of the signal. The overall signal may cover a wide frequency spectrum, but unique stages such as early inspiral, late inspiral, and merger display distinct frequency characteristics. Therefore, we utilize different sampling frequencies for the corresponding denoising models to address the specific needs of each stage.

II. DATA FOR TRAINING AND TESTING

The Einstein Telescope will be composed of three detectors positioned in a triangular layout, thereby enabling the simultaneous collection of three detectors strain data streams. In this work we only focus on one detector. We utilize the PyCBC package [60–64] to synthesize data for training, validation, and testing purposes. The strain $s(t)$ obtained by the detector can be modeled

as

$$s(t) = h(t) + n(t), \quad (1)$$

where $h(t)$ denotes the GW signal and $n(t)$ denotes the background noise. $h(t)$ can be obtained by a linear combination of $h_+(t)$ and $h_\times(t)$ that can be simulated using physical models. In this work, we use IMRPhe-nomD_NRTidal to generate $h_+(t)$ and $h_\times(t)$. For the simulation, we established a distance of 100 Mpc between the Earth and the BNS source. During the training phase, we adjusted the amplitude of $h(t)$ to attain a randomly sampled target SNR falling within the range of 20 to 40. The masses of the two neutron stars in the BNS system were randomly selected from the interval of $(1M_\odot, 2M_\odot)$, while their dimensionless spins were sampled randomly between 0 and 0.998. The right ascension and declination angles were chosen from a uniform distribution across a sphere. We cut each signal to 100 seconds duration. The signals are sampled at a rate of 8192Hz. The noise was produced through the application of the power spectrum density (PSD) associated with the Einstein Telescope. This PSD serves as an indicator of the detector's design sensitivity. Specifically, we relied on the PSD designated as EinsteinTelescopeP1600143 to create the noise. Fig. 1 illustrates the variation of amplitude spectrum density (ASD, which is the square root of PSD) with respect to frequency. For comparative purposes, the ASD curves for advanced LIGO (specifically, aLIGOZeroDetHighPower) and advanced Virgo (AdvVirgo) are also displayed alongside.

We organize our data using data packages, where each package contains one noise sample lasting 256 seconds and ten signal samples, each lasting 100 seconds. In total, we have generated 30,000 such packages, with 24,000 designated for training, 3,000 for validation, and the remaining 3,000 for testing. During the training stage, every sample is produced through instant synthesis by randomly selecting a signal, sliding it randomly, adjusting the SNR randomly, and finally, combining it with a randomly chosen noise slice. Consequently, each package has the capability to generate thousands of distinct samples for training purposes.

III. DEEP LEARNING FRAMEWORK FOR THE BNS WAVEFORM CONSTRUCTION

In this section, the proposed method for BNS waveform construction will be systematically introduced. We segment the entire time scale into numerous smaller channels, enabling each denoising model to concentrate solely on the response within its designated channel. This strategy is inspired by the SPIIR matched filtering pipeline. The diagram illustrating SPIIR for matched filtering and our proposed denoising framework (waveform construction) is presented in Fig. 2. In SPIIR, the waveform

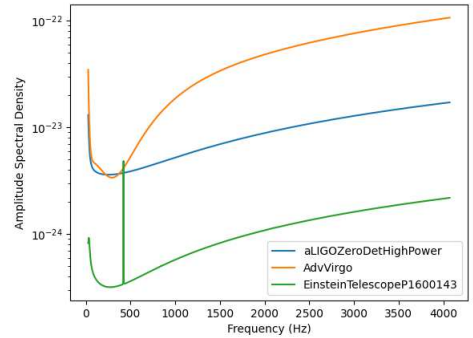


FIG. 1: The ASD curves of Einstein Telescope, Advanced LIGO and Advanced Virgo.

is estimated by adding up time-shifted, exponentially increasing sinusoids, which are formed using single-pole IIR filters. In contrast, our method estimates the waveform by summing the denoised outputs of time-shifted segments. Initially, for both SPIIR and our approach, the input signal is divided into multiple channels. Each channel i undergoes a specific time delay of d_i . In SPIIR, the time-delayed channel i subsequently passes through the respective IIR filter (IIR $_i$). The IIR filters' outputs are then aggregated to determine the SNR output.

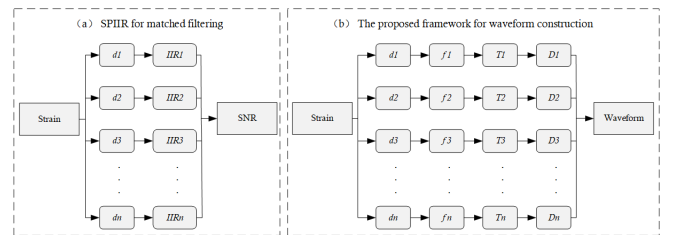


FIG. 2: A schematic of the SPIIR method and the proposed method. d_i denotes the time delay of the i th channel, f_i signifies the cut-off frequency of the low-pass filter, T_i represents the sampling period, and D_i designates the i th denoising model.

In our method, the i -th time-delayed channel is processed through a Butterworth low-pass filter with a cutoff frequency of f_i . Subsequently, the filtered strain from the i -th channel is resampled using a sampling period of T_i , where the relationship between T_i and f_i is defined as $2f_i = 1/T_i$. The resampled strain is then fed into the corresponding denoising process. Finally, the waveform is reconstructed from the outputs of the denoising process. Fig. 3 illustrates the process of combining denoised outputs to construct the final waveform. In this article, we utilize three channels as an illustrative example to explore the process of constructing BNS waveforms. The first channel is dedicated to the early inspiral stage, the second channel centers on the later inspiral stage, while the third channel concentrates on the near merger stage. These three stages correspond to three unique denoising

processes, specifically Process I, Process II, and Process III. Each process consists of a denoising model and an amplitude regularity model. Suppose the input of the denoising process of channel i is $s^i = n^i + h^i$, where $h^i \in R^{40960}$ denotes the buried signal. The denoising process can be formulated as follows

$$\hat{h}_D^i = \text{Denoise}_i(s^i | W_{D,i}), \quad (2)$$

$$\hat{h}^i = \text{Amplitude}_i(\hat{h}_D^i | W_{A,i}), \quad (3)$$

where $W_{D,i}$ and $W_{A,i}$ are the trainable parameters of the corresponding denoising model and amplitude regularity model respectively and can be optimized by

$$W_{D,i} = \underset{W_{D,i}}{\operatorname{argmin}} \text{MSE}(\hat{h}_D^i, h^i). \quad (4)$$

$$W_{A,i} = \underset{W_{A,i}}{\operatorname{argmin}} \text{MSE}(\hat{h}^i, h^i). \quad (5)$$

TABLE I: The sampling frequency, time duration of the three denoising models

Denoising process	Sampling frequency	Time duration	Input/output shape
Process I	512 Hz	80 s	R^{40960}
Process II	2048 Hz	20 s	R^{40960}
Process III	8192 Hz	5 s	R^{40960}

The structures of the models of each processes are the same, differences are the sampling frequency and time duration and these information of the three models are shown in Table I. The structure of denoising model, amplitude regularity model will be detailed in the following subsections.

A. Denoising model

The structure of the denoising model is illustrated in Fig. 4, and it consists of an Encoder-Decoder Module and a Feed-forward Network. The Encoder Module is made up of 4 Encoder blocks, 1 ResNet block, and 1 Bridge block, while the Decoder Module comprises 4 Decoder blocks, 1 Bridge block, and 1 Transformer block. In the subsequent sections, we will delve into the specifics of the Encoder, Bridge, Transformer, and Decoder blocks.

1. Encoder block

The role of the Encoder is to extract features from the input data in the network. This is achieved

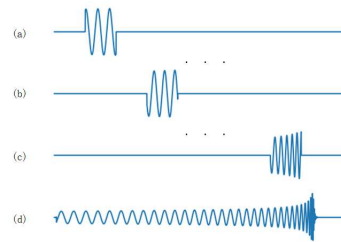


FIG. 3: An illustrative diagram presents the capability of constructing the final waveform using denoised outputs. The top three panels, labeled (a), (b), and (c), exhibit three instances of denoised outputs. Panel (d) displays the resulting constructed waveform. Please bear in mind that this figure serves solely as a visual aid for explanation.

through a ResNet block, followed by a Max-pooling layer (*Maxpooling*). The ResNet block consists of two Convolutional layers and a Residual connection. Each Convolutional layer comprises of a Convolutional (*Conv*), a Batch Normalization (*BatchNorm*), and an Exponential Linear Unit (*ELU*) activation function. The structure of the ResNet block can be formalized as

$$X'_i = \text{ELU}(\text{BatchNorm}(\text{Conv}_{(r_{in}, r_{out})}(X_{i-1}))), \quad (6)$$

$$X''_i = \text{ELU}(\text{BatchNorm}(\text{Conv}_{(r_{out}, r_{out})}(X'_i))), \quad (7)$$

$$X_i = \text{Maxpooling}(X''_i \oplus \text{Conv}_{(r_{in}, r_{out})}(X_{i-1})), \quad (8)$$

Where X_i represents the output of the i -th Encoder block. X'_i and X''_i represent the intermediate features of each ResNet block. r_{in} and r_{out} denote the number of input channels and output channels, respectively. We stipulate that the sizes of convolutional kernels, filters, strides and maxpooling are specified as follows: $\{(64, 64, 32, 32, 16), (32, 64, 128, 256, 512), 1, 2\}$.

2. Bridge block

We have additionally designed Bridge blocks to connect the UNet and Transformer. The purpose of Bridge I is to reduce the number of channels in the features in order to save computational resources. The role of Bridge II is to create skip connection that simultaneously preserves the output features of both the Encoder and Transformer, while also restoring the number of channels. The structure of the Bridge blocks can be formalized as

$$X_{b1} = \text{ELU}(\text{BatchNorm}(\text{Conv}_{(b1_{in}, b1_{out})}(X_5))), \quad (9)$$

$$X'_{b2} = \text{Conv}_{(b2_{in}, b2_{out})}(\text{Concatenate}(X_5, X_t)), \quad (10)$$

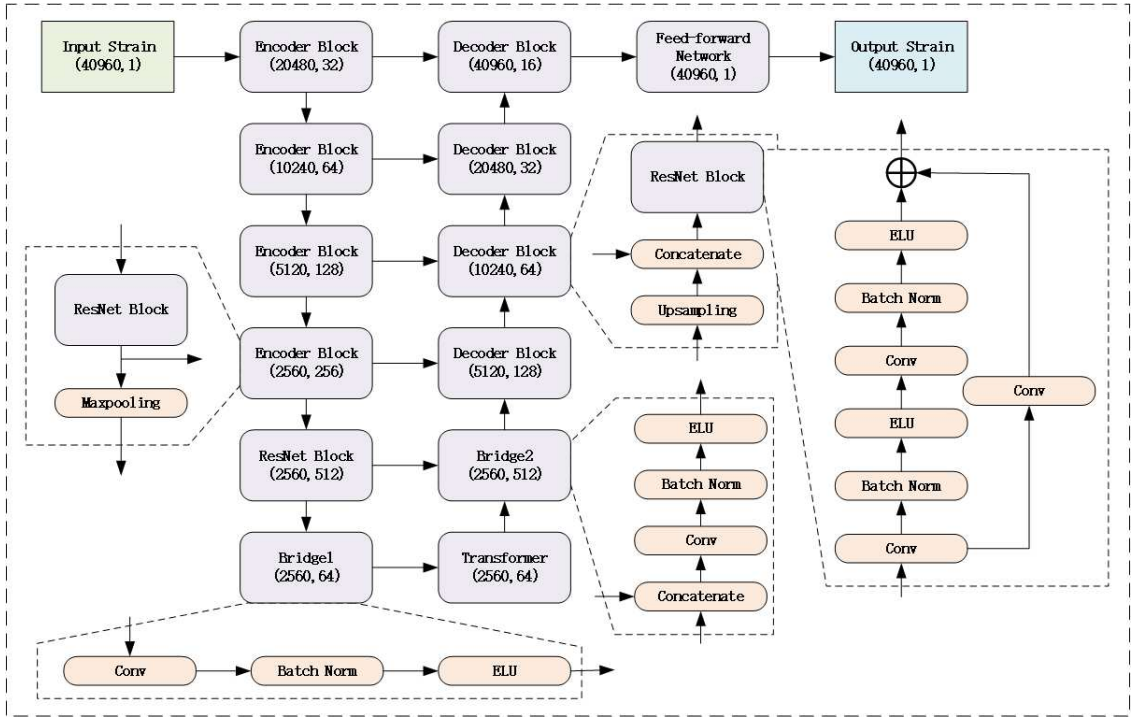


FIG. 4: The network structure of the Denoising model in the current work. The wide boxes refer to individual operations, while the narrow boxes represent sets of multiple operations. The parentheses below the boxes indicate the output dimensions of the operation group, representing the dimension of a single data point and the number of channels, respectively. The XOR symbol represents a residual structure.

$$X_{b2} = ELU(BatchNorm(X'_{b2})), \quad (11)$$

Where X_{b1} and X_{b2} respectively represent the output of Bridge I and Bridge II. X'_{b2} represents the intermediate feature of Bridge II block. X_t represents the output of Transformer. Akin to r_{in} and r_{cout} , $b1_{in}$, $b1_{cout}$, $b2_{in}$ and $b2_{cout}$ denote the input and output channels of each Bridge block. The skip connection is referred as $Concatenate(\cdot)$. We stipulate that the sizes of convolutional kernel, filters, strides and maxpooling are specified as follows: $\{(1, 16), (64, 512), 1, 2\}$.

3. Transformer block

BNS signal is a long-term sequential signal, and capturing its long-term dependencies is a key focus in denoising research. The self-attention mechanism of the Transformer can effectively capture long-term dependency relationships. The self-attention mechanism computes interaction relationships between time slices, aggregates them as output, and can dynamically aggregate relevant features based on input content, effectively capturing long-range correlations. This is why we introduce the Transformer after the Encoder. The structure of the Transformer we used is shown in Fig. 5.

To prevent overfitting of the model, we add Dropout in the Transformer. The structure of the Transformer blocks can be formalized as

$$X'_{(t,i)} = MHA(LayerNorm((X_{(t,i-1)}))), \quad (12)$$

$$X''_{(t,i)} = Dropout(X'_{(t,i)}) \oplus X_{(t,i-1)}, \quad (13)$$

$$X'''_{(t,i)} = MLP(LayerNorm((X''_{(t,i)}))), \quad (14)$$

$$X_{(t,i)} = Dropout(X'''_{(t,i)}) \oplus X''_{(t,i)}, \quad (15)$$

Where $X_{(t,i)}$ represents the output of i -th Transformer block, and $X'_{(t,i)}$, $X''_{(t,i)}$, $X'''_{(t,i)}$ represent intermediate features of the i -th Transformer block. Additionally, $LayerNorm(\cdot)$ is the operation of Layer Normalization. $MHA(\cdot)$ refers to Multi-head attention and the details are detailed in [65]. We respectively specify the number of Transformer blocks, Attention Heads, and Dropout rate as 3, 4, and 0.1. For the MLP , we follow a two-layer linear transformation structure with a Rectified Linear Unit(ReLU) activation function between the two layers. The units of the linear layer is specified as 128.

4. Decoder block

The Decoder is used to upsample the encoded features and reconstruct them back to the input strain

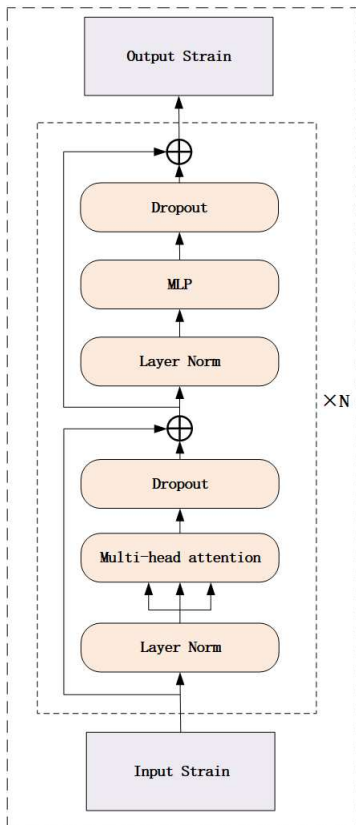


FIG. 5: The network structure of the transformer. N represents the number of blocks in the Transformer architecture.

size, providing sufficient signal reconstruction information for the Feed-forward Network. The structure of the Decoder consists of upsampling, skip connections, and residual convolutions. The Decoder first upsamples the output features from the previous layer, then connects it with the output from the same layer of the Encoder, and finally passes through a residual convolution structure identical to that of the Encoder. We stipulate that the sizes of convolutional kernels, filters, strides and upsampling are specified as follows: $\{(32, 32, 64, 64), (128, 64, 32, 16), 1, 2\}$.

5. Feed-forward Network

The Feed-forward Network obtains signal information from the Decoder and reconstructs the waveform. The structure of the Feed-forward Network we used is shown in Fig. 6. We stipulate that the sizes of convolutional kernels, filters, and strides are specified as follows: $\{(32, 32, 16, 16), (32, 16, 8, 1), 1\}$.

B. Amplitude Regularity model

When we test our denoising model in practice, we observe that the denoised results often exhibit amplitude reduction in certain areas. To optimize the local structure of the waveform, we prune the denoising model and construct a new architecture, which we call the Amplitude Regularity Model. This model removes the Transformer and Bridge components and adjusts the pooling and upsampling dimensions to 4. The network structure of Amplitude Regularity Model is shown in FIG. 7.

C. Waveform construction method

After the previous deep learning processing, we obtain three denoised waveforms (Waveform 1, Waveform 2, and Waveform 3) for different channels with sampling rates of 512 Hz, 2048 Hz, and 8192 Hz, respectively. In this subsection, we detail the waveform construction method. The construction method shown in Fig 8, takes Waveform 1, Waveform 2, and Waveform 3 as input and Constructed Waveform as output. Due to the varying sampling frequencies of each denoised waveform, Waveform 1 and Waveform 2 must undergo upsampling to 8192 Hz prior to their combination. For the upsampling process, spline interpolation is utilized. Suppose the upsampled Waveform 1, Waveform 2 and Waveform 3 can be denote as $h_1(t)$, $h_2(t)$ and $h_3(t)$. The amplitudes of the three waveforms may not be aligned, thus necessitating amplitude adjustments prior to their combination. Specifically, we must adjust the amplitude of $h_2(t)$ to match that of $h_3(t)$, and similarly, adapt the amplitude of $h_1(t)$ to align with the adapted $h_2(t)$.

Here, we introduce the combination of $h_1(t)$, $h_2(t)$ and $h_3(t)$. We initially add zeroes to the three waveforms to ensure that they all possess the same length. Define the function $I_{ij}(t)$ (refer to Eq. (16)) which can ascertain whether waveforms i and j exhibit any temporal overlap.

$$I_{ij}(t) = \begin{cases} 1, & h_i \text{ and } h_j \text{ at time } t \text{ are overlap} \\ 0, & \text{otherwise} \end{cases} \quad (16)$$

We then normalize $h_2(t)$ to $\bar{h}_2(t)$ by

$$\bar{h}_2(t) = \frac{\sqrt{\int h_3^2(t) I_{23}(t) dt}}{\sqrt{\int h_3^2(t) I_{23}(t) dt}} h_2(t). \quad (17)$$

We then normalize $h_1(t)$ to $\bar{h}_1(t)$ by

$$\bar{h}_1(t) = \frac{\sqrt{\int \bar{h}_2^2(t) I_{12}(t) dt}}{\sqrt{\int h_1^2(t) I_{12}(t) dt}} h_1(t). \quad (18)$$

We then construct the waveform $h(t)$ by

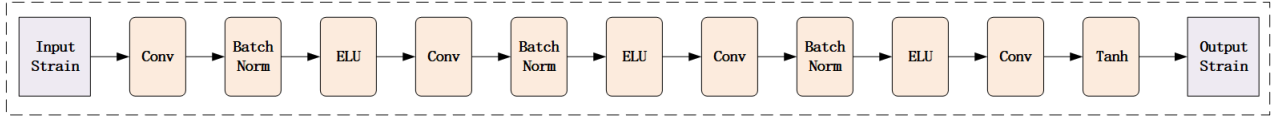


FIG. 6: The network structure of the Feed-forward Network

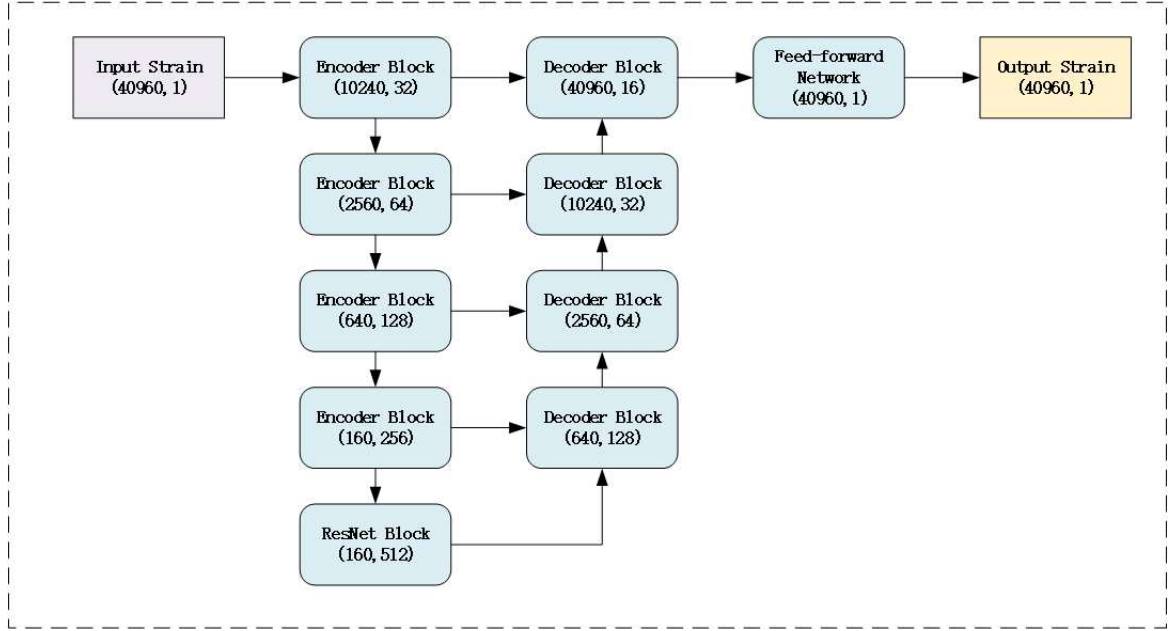


FIG. 7: The network structure of the Amplitude Regularity model. It is similar to the Denoising model, but removes the Transformer and Bridge structures, and increases the pooling size to 4.

$$\begin{aligned} h(t) &= h'(t) - h''(t) \\ &= h'(t) \left[1 - \frac{1}{2}I_{12}(t) - \frac{1}{2}I_{23}(t) \right], \end{aligned} \quad (19)$$

where $h'(t)$ and $h''(t)$ are defined as

$$h'(t) = [\bar{h}_1(t) + \bar{h}_2(t) + h_3(t)]. \quad (20)$$

$$\begin{aligned} h''(t) &= \frac{\bar{h}_1(t) + \bar{h}_2(t)}{2} I_{12}(t) + \frac{\bar{h}_2(t) + h_3(t)}{2} I_{23}(t) \\ &= \frac{\bar{h}_1(t) + \bar{h}_2(t) + h_3(t)}{2} (I_{12}(t) + I_{23}(t)). \end{aligned} \quad (21)$$

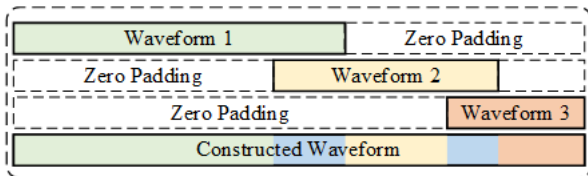


FIG. 8: The diagram of waveform construction

IV. THE PERFORMANCE OF BNS WAVEFORM RECONSTRUCTION

Three models, namely Model I, Model II, and Model III, were trained using the training dataset. Each model specializes in a specific stage: Model I focus on the waveform extraction of early inspiral stage, Model II on the waveform extraction of late inspiral stage, and Model III on the waveform extraction of near merger stage. In this section, we evaluate the performance of all three models using the test dataset.

To enhance the denoising model, we have upgraded the conventional UNet framework by incorporating Transformer and bridge elements to the feature output of the final Encoder Module. Additionally, we trained three Amplitude Regularity Models to facilitate a deeper analysis of the denoising model's output. To validate the utility of both the Transformer module and Amplitude Regularity Models, we also conducted performance tests with and without the Transformer.

We use overlap of the denoised waveform and the buried signal as the evaluation metric for waveform extraction. Suppose $a(t)$ and $b(t)$ are two timeseries with aligned phases, the overlap of $a(t)$ and $b(t)$ can be calculated as follows:

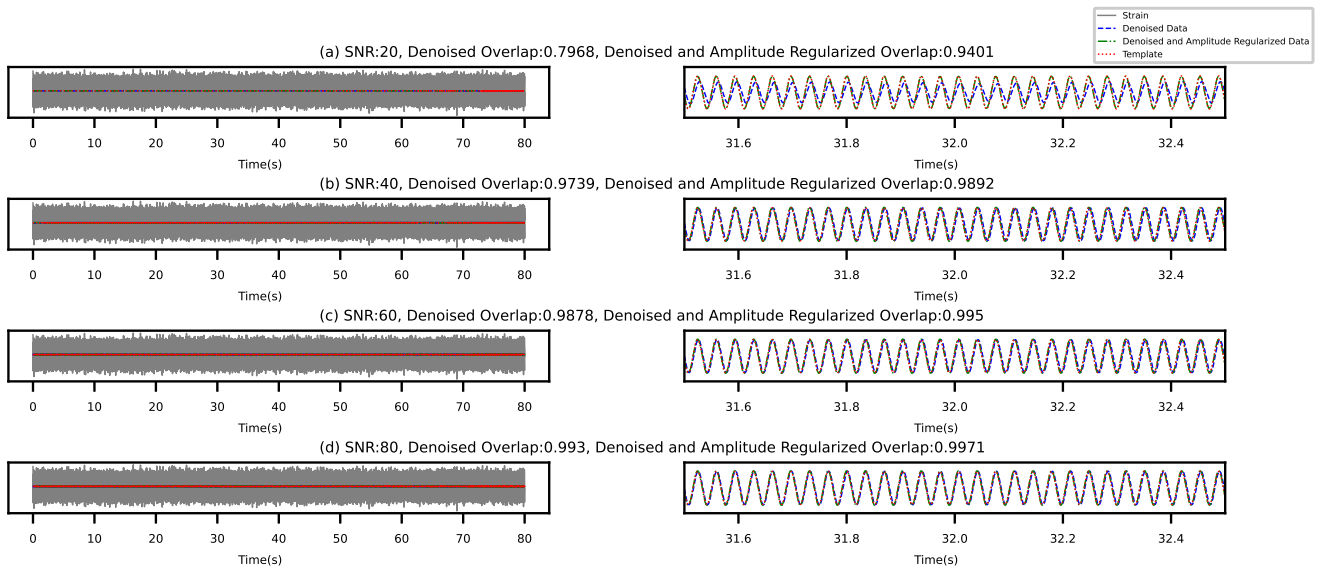


FIG. 9: The comparisons between the denoising results and the signal on the early inspiral stage, at SNRs of 20, 40 60 80 sequentially.

$$\text{overlap}(a, b) = \frac{\int a(t)b(t)dt}{\sqrt{\int a^2(t)dt \int b^2(t)dt}}. \quad (22)$$

Please note that Eq. (22) differs from its counterpart in previous works [51, 52], and it has the capability to reflect both the phase alignment and amplitude variation of two signals. By computing the overlap metric, we can evaluate the model’s denoising performance on the test datasets. The closer the metric is to 1, the more effectively the model can remove noise while retaining the BNS events from the original datasets. A lower metric indicates that the model may lose some original data during the denoising process.

For each waveform in the test dataset (30,000 waveforms), we initially normalized it to a randomly selected SNR value falling within the range of 20 to 80. Subsequently, we randomly trimmed the background noise and constructed the strain with combine of the signal and noise.

A. Performance of waveform extraction on the early inspiral stage

We initially processed each combined strain of test data by passing it through a low-pass filter set at a cut-off frequency of 256 Hz. Following this, we resampled the strain data at a frequency of 512 Hz. Next, we randomly selected an 80-second segment of the resampled strain, ensuring that its endpoint preceded the merger time by 15 to 18 seconds. Subsequently, we fed this 80-second segment into Model I and obtained the output.

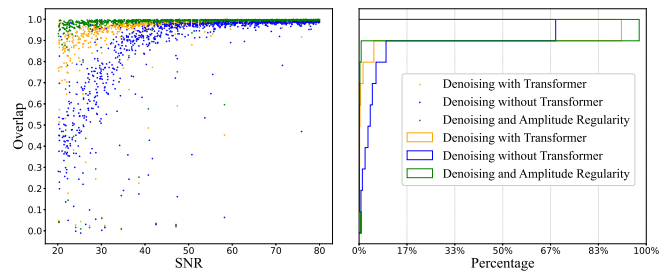


FIG. 10: The overlap of the denoised output and the buried signal in test dataset on the early inspiral stage.

The comparisons between the extracted results and the underlying signal of a randomly chosen resampled strain at various SNRs of 20, 40, 60, and 80 are presented in Fig. 9. As depicted in Fig. 9, at a SNR of 20, relying solely on the denoising model incorporating the Transformer leads to notable waveform distortion. Nevertheless, once the denoised signal is processed through the amplitude regularity model, the waveform is rectified, aligning more closely with the template. For SNRs exceeding 40, the substantial distortion in the denoised waveform diminishes significantly, regardless of whether the amplitude regularity model is employed. Macroscopically, there is no discernible difference in waveform distortion.

In Fig. 10, we illustrate the overlap distribution between the extracted early inspiral waveform and the buried template. For comparison, we also depict the corresponding overlap distributions of the outputs from denoising models, comparing those with and without the inclusion of the Transformer module. In the absence of the Transformer module, only approximately 70% of

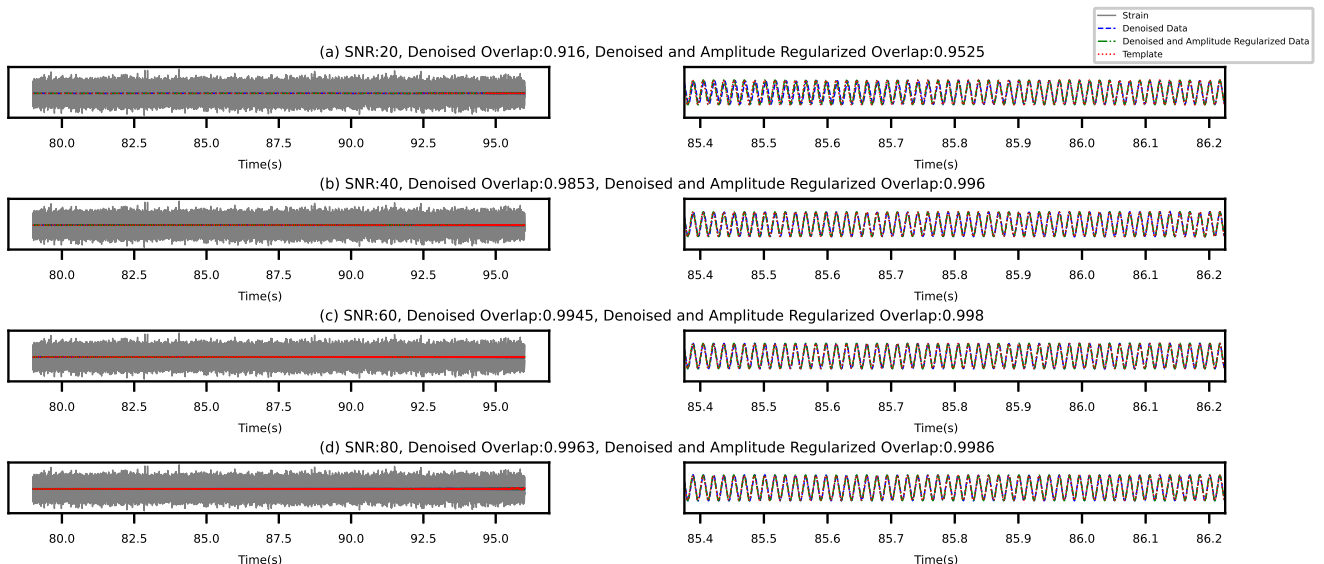


FIG. 11: The comparisons between the denoising results and the signal on the late inspiral stage, at SNRs of 20, 40 60 80 sequentially.

the samples exhibited an overlap exceeding 90%. However, the introduction of the Transformer module significantly enhanced denoising performance, increasing the 90% overlap percentage from 70% to 90%. Furthermore, when the Amplitude Regularity Model was incorporated, the waveform extraction performance rose further, the 90% overlap percentage increased about 5%. It is evident that the Transformer structure plays a pivotal role in significantly elevating the denoising capabilities of the model. Moreover, the Amplitude Regularity Model proves to be indispensable within our framework, exhibiting notable benefits, especially under low signal-to-noise ratio conditions.

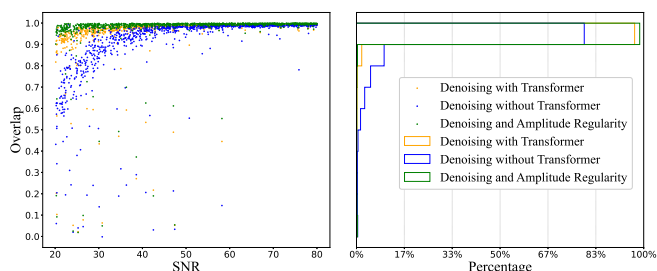


FIG. 12: The overlap of the denoised output and the buried signal in test dataset on the late inspiral stage.

B. Performance of waveform extraction on the late inspiral stage

In this subsection, akin to the preceding one, we conduct experiments aimed at evaluating the performance

of Model II in waveform extraction. Initially, we applied a 1024 Hz low-pass filter to the combined strain, subsequently resampling it at a 2048 Hz frequency. Following this preprocessing step, we randomly cut the late inspiral part (the merger time being after the end time of the time slice about 1 s to 2 s) and proceeded to extract the buried signal.

Fig. 11 presents an example of the extracted output juxtaposed with the buried template. Evidently, in the denoising-only scenario at SNR 20, the overlap stands at 91.6%. However, when we feed the denoised output into the Amplitude Regularity Model, the overlap is significantly enhanced to 95.25%, marking an improvement of approximately 4%. Akin to Fig. 10, we have also analyzed the overlap distribution of Model II, as depicted in Fig. 12. In the late inspiral case, both the transformer and amplitude regularity models prove crucial for effective waveform extraction.

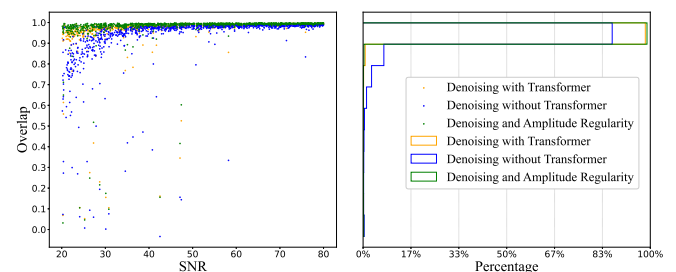


FIG. 13: The overlap of the denoised output and the buried signal in test dataset near merger.

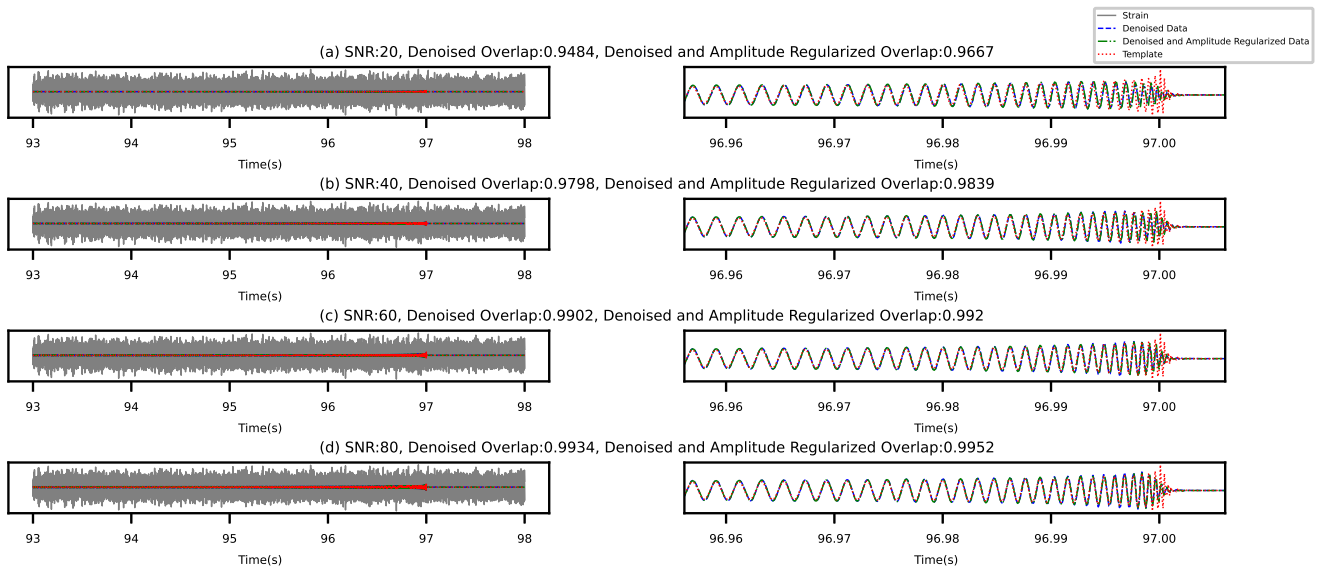


FIG. 14: The comparisons between the denoising results and the signal ner merger, at SNRs of 20, 40 60 80 sequentially.

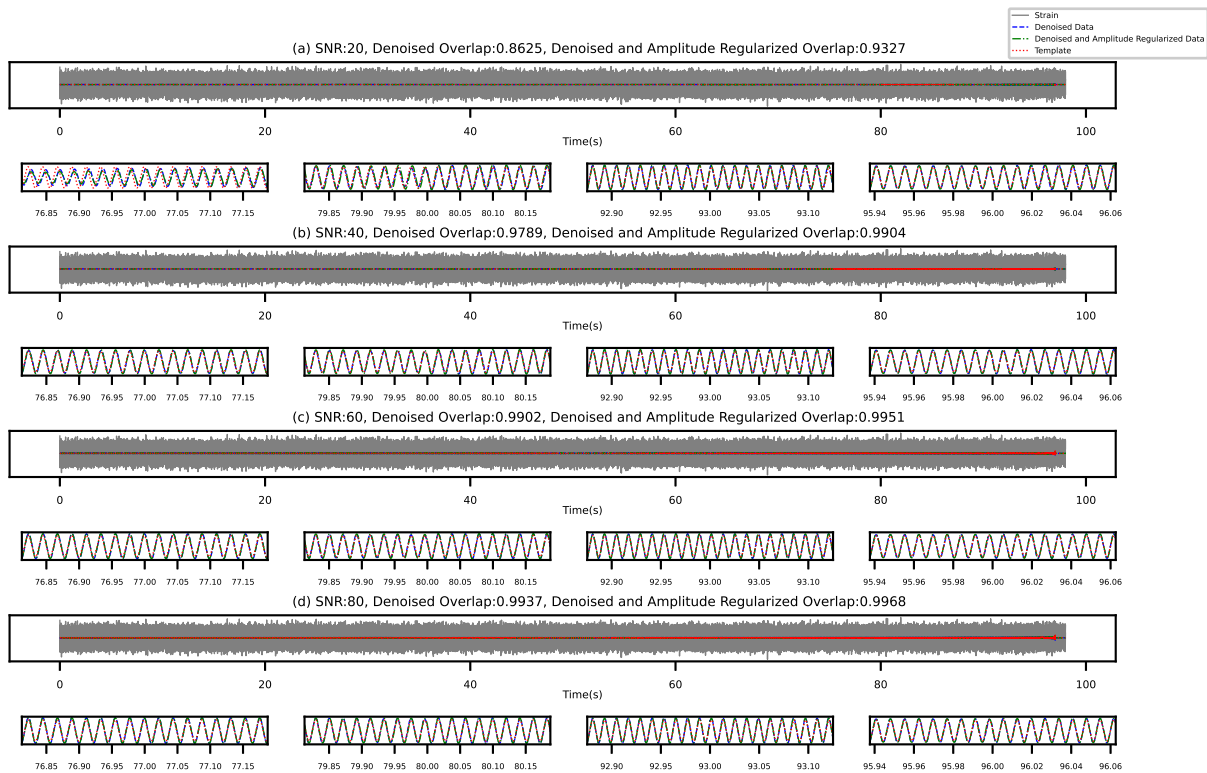


FIG. 15: The comparisons between the denoising results and the signal after restructuring, at SNRs of 20, 40 60 80 sequentially.

C. Performance of waveform extraction near merger

We have previously analyzed the performance of waveform extraction during the early and late inspiral stages.

In this subsection, we focus our attention on the waveform extraction performance specifically near the merger phase. To assess this, for each strain, we cut a 5-second segment containing merger phase, with the merger time occurring randomly between 3 to 4 seconds within the

segment. We then extract the waveform from the selected segment to evaluate its performance.

As shown in Fig. 13 and Fig. 14, the model exhibits performance similar to the preceding two inspiral periods before the merging time. However, during the peak interval of merging, the amplitude of the denoised signal fails to keep pace with the drastic changes in the template waveform, potentially resulting in premature attenuation of amplitude. This amplitude decay is more likely to occur under low SNR conditions.

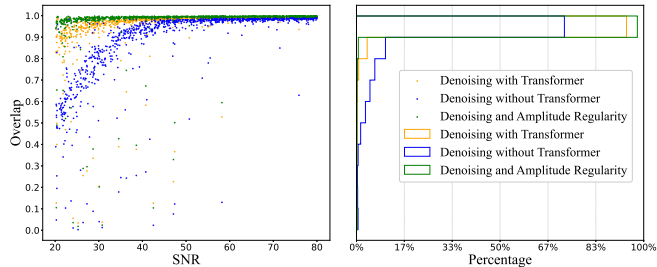


FIG. 16: The overlap of the denoised output and the buried signal in test dataset for the whole BNS signal.

D. Performance of reconstruction the whole 100 seconds length BNS signal

At this stage, we reconstruct the data from the previous three stages into the original data and investigate the overall denoising effect. As depicted in Fig. 15 and Fig. 16, this is a 98 second synthetic signal with overlapped positions between 77 to 80 seconds and 93 to 96 seconds. We also present waveform overlapped information for four overlapped edge positions. The results show that the designed waveform reconstruction method effectively integrate our segmented denoising results without

sudden waveform fluctuations at the overlapped edge. It also adheres to the overall overlap observed in the previous three testing phases.

V. CONCLUSION AND DISCUSSION

In conclusion, this study has presented a novel approach for BNS waveform extraction utilizing deep learning techniques. Through rigorous experimentation and analysis, we have demonstrated the effectiveness of our proposed method in addressing the challenges associated with processing GW data from ET. The proposed framework, inspired by the SPIIR method for matched filtering, combines denoising outputs of time-delayed strain to reconstruct the embedded BNS waveform. We have constructed three distinct denoising models, each tailored to specific phases of the BNS GW: early inspiral, later inspiral, and merger. We add Transformer encoder module to the Unet structured denoising model. We have conducted experiments to compare the denoising performance of the model both with and without the Transformer. The results demonstrate that the model incorporating the Transformer outperforms the one without it. We have also introduced the Amplitude Regularity Model, and experimental results indicate that this model can further enhance waveform extraction performance. We believe that our proposed method holds significant potential for early warning, searching, and localization of BNS GWs. Looking ahead, we anticipate that further refinements and extensions of our method could enhance its accuracy and reliability, ultimately contributing to a more comprehensive understanding of gravitational waves and their sources. We hope that our work will inspire future research in this exciting and rapidly developing field.

-
- [1] Ethan Marx, William Benoit, Alec Gunny, Rafia Omer, Deep Chatterjee, Ricco C Venterea, Lauren Wills, Muhammed Saleem, Eric Moreno, Ryan Raikman, et al. A machine-learning pipeline for real-time detection of gravitational waves from compact binary coalescences. *arXiv preprint arXiv:2403.18661*, 2024.
- [2] Benjamin P Abbott, Richard Abbott, TDea Abbott, S Abraham, F Acernese, K Ackley, C Adams, RX Adhikari, VB Adya, Christoph Affeldt, et al. Gwtc-1: a gravitational-wave transient catalog of compact binary mergers observed by ligo and virgo during the first and second observing runs. *Physical Review X*, 9(3):031040, 2019.
- [3] Richard Abbott, TD Abbott, S Abraham, F Acernese, K Ackley, A Adams, C Adams, RX Adhikari, VB Adya, Christoph Affeldt, et al. Gwtc-2: compact binary coalescences observed by ligo and virgo during the first half of the third observing run. *Physical Review X*, 11(2):021053, 2021.
- [4] R Abbott, TD Abbott, F Acernese, K Ackley, C Adams, N Adhikari, RX Adhikari, VB Adya, C Affeldt, D Agarwal, et al. Gwtc-2.1: Deep extended catalog of compact binary coalescences observed by ligo and virgo during the first half of the third observing run. *Physical Review D*, 109(2):022001, 2024.
- [5] Richard Abbott, TD Abbott, F Acernese, K Ackley, C Adams, N Adhikari, RX Adhikari, VB Adya, C Affeldt, D Agarwal, et al. Gwtc-3: compact binary coalescences observed by ligo and virgo during the second part of the third observing run. *Physical Review X*, 13(4):041039, 2023.
- [6] Benjamin P Abbott, Rich Abbott, TDea Abbott, Fausto Acernese, Kendall Ackley, Carl Adams, Thomas Adams, Paolo Addresso, Rana X Adhikari, Vaishali B Adya, et al. Gw170817: observation of gravitational waves from a binary neutron star inspiral. *Physical review letters*,

- 119(16):161101, 2017.
- [7] W Hartley. Multi-messenger observations of a binary neutron star merger. *The Astrophysical Journal Letters*, 848(2):L12, 2017.
- [8] Benjamin P Abbott, Robert Abbott, TD Abbott, F Acernese, K Ackley, C Adams, T Adams, P Addesso, RX Adhikari, VB Adya, et al. Gravitational waves and gamma-rays from a binary neutron star merger: Gw170817 and grb 170817a. *The Astrophysical Journal Letters*, 848(2):L13, 2017.
- [9] BP Abbott, R Abbott, TD Abbott, F Acernese, K Ackley, C Adams, T Adams, P Addesso, RX Adhikari, VB Adya, et al. Properties of the binary neutron star merger gw170817. *Physical Review X*, 9(1):011001, 2019.
- [10] Soumi De, Daniel Finstad, James M Lattimer, Duncan A Brown, Edo Berger, and Christopher M Biwer. Erratum: Tidal deformabilities and radii of neutron stars from the observation of gw170817 [phys. rev. lett. 121, 091102 (2018)]. *Physical Review Letters*, 121(25):259902, 2018.
- [11] Benjamin P Abbott, Richard Abbott, TD Abbott, F Acernese, K Ackley, C Adams, T Adams, P Addesso, Rana X Adhikari, Vaishali B Adya, et al. Gw170817: Measurements of neutron star radii and equation of state. *Physical review letters*, 121(16):161101, 2018.
- [12] Benjamin J Owen. Search templates for gravitational waves from inspiraling binaries: Choice of template spacing. *Physical Review D*, 53(12):6749, 1996.
- [13] Bruce Allen, Warren G. Anderson, Patrick R. Brady, Duncan A. Brown, and Jolien D. E. Creighton. Findchirp: an algorithm for detection of gravitational waves from inspiraling compact binaries. *Physical Review D*, 85(12):3652–3656, 2005.
- [14] Cody Messick, Kent Blackburn, Patrick Brady, Patrick Brockill, Kipp Cannon, Romain Cariou, Sarah Caudill, Sydney J Chamberlin, Jolien DE Creighton, Ryan Everett, et al. Analysis framework for the prompt discovery of compact binary mergers in gravitational-wave data. *Physical Review D*, 95(4):042001, 2017.
- [15] Florian Aubin, Francesco Brighenti, Roberto Chierici, Dimitri Estevez, Giuseppe Greco, Gianluca Maria Guidi, Vincent Juste, Frédérique Marion, Benoit Mours, Elisa Nitoglia, et al. The mbta pipeline for detecting compact binary coalescences in the third ligo–virgo observing run. *Classical and Quantum Gravity*, 38(9):095004, 2021.
- [16] Alexander H Nitz, Thomas Dent, Tito Dal Canton, Stephen Fairhurst, and Duncan A Brown. Detecting binary compact-object mergers with gravitational waves: Understanding and improving the sensitivity of the pycbc search. *The Astrophysical Journal*, 849(2):118, 2017.
- [17] Samantha A Usman, Alexander H Nitz, Ian W Harry, Christopher M Biwer, Duncan A Brown, Miriam Cabero, Collin D Capano, Tito Dal Canton, Thomas Dent, Stephen Fairhurst, et al. The pycbc search for gravitational waves from compact binary coalescence. *Classical and Quantum Gravity*, 33(21):215004, 2016.
- [18] Ian Harry, Stephen Privitera, Alejandro Bohé, and Alessandra Buonanno. Searching for gravitational waves from compact binaries with precessing spins. *Physical Review D*, 94(2):024012, 2016.
- [19] Einstein Telescope et al. Science with the einstein telescope: a comparison of different designs. *Journal of Cosmology and Astroparticle Physics*, 2023(7), 2023.
- [20] Varun Srivastava, Derek Davis, Kevin Kuns, Philippe Landry, Stefan Ballmer, Matthew Evans, Evan D Hall, Jocelyn Read, and BS Sathyaprakash. Science-driven tunable design of cosmic explorer detectors. *The Astrophysical Journal*, 931(1):22, 2022.
- [21] Teng Zhang, Huan Yang, Denis Martynov, Patricia Schmidt, and Haixing Miao. Gravitational-wave detector for postmerger neutron stars: beyond the quantum loss limit of the fabry-perot-michelson interferometer. *Physical Review X*, 13(2):021019, 2023.
- [22] Tianyu Zhao, Ruijun Shi, Yue Zhou, Zhoujian Cao, and Zhixiang Ren. Dawning of a new era in gravitational wave data analysis: Unveiling cosmic mysteries via artificial intelligence—a systematic review. *arXiv preprint arXiv:2311.15585*, 2023.
- [23] Elena Cuoco, Jade Powell, Marco Cavaglià, Kendall Ackley, Michał Bejger, Chayan Chatterjee, Michael Coughlin, Scott Coughlin, Paul Easter, Reed Essick, et al. Enhancing gravitational-wave science with machine learning. *Machine Learning: Science and Technology*, 2(1):011002, 2020.
- [24] Daniel George and Eliu Antonio Huerta. Deep learning for real-time gravitational wave detection and parameter estimation: Results with advanced ligo data. *Physics Letters B*, 778:64–70, 2018.
- [25] Hunter Gabbard, Michael Williams, Fergus Hayes, and Chris Messenger. Matching matched filtering with deep networks for gravitational-wave astronomy. *Physical review letters*, 120(14):141103, 2018.
- [26] XiLong Fan, Jin Li, Xin Li, YuanHong Zhong, and Jun-Wei Cao. Applying deep neural networks to the detection and space parameter estimation of compact binary coalescence with a network of gravitational wave detectors. *Science China Physics, Mechanics & Astronomy*, 62:1–8, 2019.
- [27] Hua-Mei Luo, Wenbin Lin, Zu-Cheng Chen, and Qing-Guo Huang. Extraction of gravitational wave signals with optimized convolutional neural network. *Frontiers of Physics*, 15:1–6, 2020.
- [28] Xiang-Ru Li, Wo-Liang Yu, Xi-Long Fan, and G Jogesh Babu. Some optimizations on detecting gravitational wave using convolutional neural network. *Frontiers of physics*, 15:1–11, 2020.
- [29] Marlin B Schäfer, Ondřej Zelenka, Alexander H Nitz, Frank Ohme, and Bernd Brügmann. Training strategies for deep learning gravitational-wave searches. *Physical Review D*, 105(4):043002, 2022.
- [30] Marlin B Schäfer, Ondřej Zelenka, Alexander H Nitz, He Wang, Shichao Wu, Zong-Kuan Guo, Zhoujian Cao, Zhixiang Ren, Paraskevi Nousi, Nikolaos Stergioulas, et al. First machine learning gravitational-wave search mock data challenge. *Physical Review D*, 107(2):023021, 2023.
- [31] Timothy D Gebhard, Niki Kilbertus, Ian Harry, and Bernhard Schölkopf. Convolutional neural networks: A magic bullet for gravitational-wave detection? *Physical Review D*, 100(6):063015, 2019.
- [32] Wei Wei, Asad Khan, EA Huerta, Xiaobo Huang, and Minyang Tian. Deep learning ensemble for real-time gravitational wave detection of spinning binary black hole mergers. *Physics Letters B*, 812:136029, 2021.
- [33] EA Huerta, Asad Khan, Xiaobo Huang, Minyang Tian, Maksim Levental, Ryan Chard, Wei Wei, Maeve Heflin, Daniel S Katz, Volodymyr Kindratenko, et al. Accelerated, scalable and reproducible ai-driven gravitational

- wave detection. *Nature Astronomy*, 5(10):1062–1068, 2021.
- [34] CunLiang Ma, Wei Wang, He Wang, and Zhoujian Cao. Ensemble of deep convolutional neural networks for real-time gravitational wave signal recognition. *Physical Review D*, 105(8):083013, 2022.
- [35] Seiya Sasaoka, Naoki Koyama, Diego Dominguez, Yusuke Sakai, Kentaro Somiya, Yuto Omae, and Hirotaaka Takahashi. Comparative study of 1d and 2d convolutional neural network models with attribution analysis for gravitational wave detection from compact binary coalescences. *Physical Review D*, 109(4):043011, 2024.
- [36] Yuewei Zhang, Haiguang Xu, Meilin Liu, Cheng Liu, Yuanyuan Zhao, and Jie Zhu. Deep learning model based on a bidirectional gated recurrent unit for the detection of gravitational wave signals. *Physical Review D*, 106(12):122002, 2022.
- [37] He Wang, Shichao Wu, Zhoujian Cao, Xiaolin Liu, and Jian-Yang Zhu. Gravitational-wave signal recognition of ligo data by deep learning. *Physical Review D*, 101(10):104003, 2020.
- [38] Plamen G Krastev. Real-time detection of gravitational waves from binary neutron stars using artificial neural networks. *Physics Letters B*, 803:135330, 2020.
- [39] Plamen G Krastev, Kiranjyot Gill, V Ashley Villar, and Edo Berger. Detection and parameter estimation of gravitational waves from binary neutron-star mergers in real ligo data using deep learning. *Physics Letters B*, 815:136161, 2021.
- [40] Margherita Fasano, Kaze WK Wong, Andrea Maselli, Emanuele Berti, Valeria Ferrari, and Bangalore S Sathyaprakash. Distinguishing double neutron star from neutron star-black hole binary populations with gravitational wave observations. *Physical Review D*, 102(2):023025, 2020.
- [41] João Aveiro, Felipe F Freitas, Márcio Ferreira, Antonio Onofre, Constança Providência, Gonçalo Gonçalves, and José A Font. Identification of binary neutron star mergers in gravitational-wave data using object-detection machine learning models. *Physical Review D*, 106(8):084059, 2022.
- [42] Chayan Chatterjee and Linqing Wen. Premerger sky localization of gravitational waves from binary neutron star mergers using deep learning. *The Astrophysical Journal*, 959(2):76, 2023.
- [43] Wei Wei, EA Huerta, Mengshen Yun, Nicholas Loutrel, Md Arif Shaikh, Prayush Kumar, Roland Haas, and Volodymyr Kindratenko. Deep learning with quantized neural networks for gravitational-wave forecasting of eccentric compact binary coalescence. *The Astrophysical Journal*, 919(2):82, 2021.
- [44] Marlin B Schäfer, Frank Ohme, and Alexander H Nitz. Detection of gravitational-wave signals from binary neutron star mergers using machine learning. *Physical Review D*, 102(6):063015, 2020.
- [45] Grégory Baltus, Justin Janquart, Melissa Lopez, Amit Reza, Sarah Caudill, and Jean-René Cudell. Convolutional neural networks for the detection of the early inspiral of a gravitational-wave signal. *Physical Review D*, 103(10):102003, 2021.
- [46] Hang Yu, Rana X Adhikari, Ryan Magee, Surabhi Sachdev, and Yanbei Chen. Early warning of coalescing neutron-star and neutron-star-black-hole binaries from the nonstationary noise background using neural networks. *Physical Review D*, 104(6):062004, 2021.
- [47] Grégory Baltus, Justin Janquart, Melissa Lopez, Harsh Narola, and Jean-René Cudell. Convolutional neural network for gravitational-wave early alert: Going down in frequency. *Physical Review D*, 106(4):042002, 2022.
- [48] Leo P Singer and Larry R Price. Rapid bayesian position reconstruction for gravitational-wave transients. *Physical Review D*, 93(2):024013, 2016.
- [49] Cunliang Ma, Wei Wang, He Wang, and Zhoujian Cao. Artificial intelligence model for gravitational wave search based on the waveform envelope. *Physical Review D*, 107(6):063029, 2023.
- [50] CunLiang Ma, Sen Wang, Wei Wang, and Zhoujian Cao. Using deep learning to predict matched signal-to-noise ratio of gravitational waves. *Physical Review D*, 109(4):043009, 2024.
- [51] Wei Wei and EA Huerta. Gravitational wave denoising of binary black hole mergers with deep learning. *Physics Letters B*, 800:135081, 2020.
- [52] Chayan Chatterjee, Linqing Wen, Foivos Diakogiannis, and Kevin Vinsen. Extraction of binary black hole gravitational wave signals from detector data using deep learning. *Physical Review D*, 104(6):064046, 2021.
- [53] He Wang, Yue Zhou, Zhoujian Cao, Zong-Kuan Guo, and Zhixiang Ren. Waveformer: transformer-based denoising method for gravitational-wave data. *Machine Learning: Science and Technology*, 2024.
- [54] Chayan Chatterjee and Karan Jani. Reconstruction of binary black hole harmonics in ligo using deep learning. *arXiv preprint arXiv:2403.01559*, 2024.
- [55] Vicky Kalogera, BS Sathyaprakash, Matthew Bailes, Marie-Anne Bizouard, Alessandra Buonanno, Adam Burrows, Monica Colpi, Matt Evans, Stephen Fairhurst, Stefan Hild, et al. The next generation global gravitational wave observatory: the science book. *arXiv preprint arXiv:2111.06990*, 2021.
- [56] Francesco Iacovelli, Michele Mancarella, Stefano Foffa, and Michele Maggiore. Forecasting the detection capabilities of third-generation gravitational-wave detectors using gwfast. *The Astrophysical Journal*, 941(2):208, 2022.
- [57] Wathela Alhassan, Tomasz Bulik, and Mariusz Suchenek. Detection of einstein telescope gravitational wave signals from binary black holes using deep learning. *Monthly Notices of the Royal Astronomical Society*, 519(3):3843–3850, 2023.
- [58] Wathela Alhassan, T Bulik, and M Suchenek. Einstein telescope: binary black holes gravitational wave signals detection from three detectors combined data using deep learning. *arXiv preprint arXiv:2310.10409*, 2023.
- [59] Quirijn Meijer, Melissa Lopez, Daichi Tsuna, and Sarah Caudill. Gravitational-wave searches for cosmic string cusps in einstein telescope data using deep learning. *Physical Review D*, 109(2):022006, 2024.
- [60] Alexander H Nitz, Tito Dal Canton, Derek Davis, and Steven Reyes. Rapid detection of gravitational waves from compact binary mergers with pycbc live. *Physical Review D*, 98(2):024050, 2018.
- [61] Christopher Michael Biwer, Collin D Capano, Soumi De, Miriam Cabero, Duncan A Brown, Alexander H Nitz, and Vivien Raymond. Pycbc inference: A python-based parameter estimation toolkit for compact binary coalescence signals. *Publications of the Astronomical Society of the Pacific*, 131(996):024503, 2019.
- [62] Tito Dal Canton, Alexander H Nitz, Andrew P Lund-

- gren, Alex B Nielsen, Duncan A Brown, Thomas Dent, Ian W Harry, Badri Krishnan, Andrew J Miller, Karl Wette, et al. Implementing a search for aligned-spin neutron star-black hole systems with advanced ground based gravitational wave detectors. *Physical Review D*, 90(8):082004, 2014.
- [63] Alexander H Nitz, Thomas Dent, Tito Dal Canton, Stephen Fairhurst, and Duncan A Brown. Detecting binary compact-object mergers with gravitational waves: Understanding and improving the sensitivity of the pycbc search. *The Astrophysical Journal*, 849(2):118, 2017.
- [64] Bruce Allen, Warren G Anderson, Patrick R Brady, Duncan A Brown, and Jolien DE Creighton. Findchirp: An algorithm for detection of gravitational waves from inspiraling compact binaries. *arXiv preprint gr-qc/0509116*, 2005.
- [65] Ashish Vaswani, Noam Shazeer, Niki Parmar, Jakob Uszkoreit, Llion Jones, Aidan N Gomez, Lukasz Kaiser, and Illia Polosukhin. Attention is all you need. *Advances in neural information processing systems*, 30, 2017.